

Performance Analysis of a Helical Savonius Rotor with Shaft at 45° Twist Angle Using CFD

Rajat Gupta¹, Bachu Deb¹ & R. D. Misra¹

¹Department of Mechanical Engineering, NIT Silchar Silchar, Assam, India

Correspondence: Bachu Deb, Department of Mechanical Engineering, NIT Silchar, Silchar 788010, Assam, India.
Tel: 91-940-181-1970. E-mail: bachudeb@gmail.com

Received: October 19, 2012

Accepted: November 9, 2012

Online Published: February 28, 2013

doi:10.5539/mer.v3n1p118

URL: <http://dx.doi.org/10.5539/mer.v3n1p118>

Abstract

Helical Savonius rotor is considered to be superior to conventional Savonius rotor in terms of higher power coefficient (C_p) and better starting characteristic. However studies related to helical Savonius rotors is few. In view of this, in this paper, the performance of a helical Savonius rotor with shaft at 45° bucket twist angle for one complete cycle of rotation was analyzed using Computational Fluid Dynamics. A two-bucket helical Savonius rotor with shaft was designed using GAMBIT, having a height of 60 cm and diameter of 17 cm with 45° bucket twist angle. A three dimensional Computational Fluid Dynamics analysis using Fluent package was done to predict the performance of the rotor. Standard k- ϵ turbulence model with second order upwind discretization scheme and standard wall condition was used. Grid independence test was also conducted to have the best meshing accuracy. Power coefficients (C_p) of the rotor at different tip speed ratios were evaluated for rotor angle variation from 0° to 180°. C_p at each rotor angle increased with increase of tip speed ratio up to an optimum tip speed ratio, but then decreased even if tip speed ratio was further increased. Moreover, the effect of rotor angle on C_p in a complete cycle of rotation was analyzed. C_p was found to be positive at all rotor angles, and higher values of C_p were obtained at rotor angles namely 45°, 90°, 225° and 270°, which would contribute maximum power production by the rotor. In addition to these, flow physics of the rotor was studied using tangential velocity plots w.r.t. rotor angle and path lines across the rotor. It was found that at 45°, 90° and 135° rotor angles, maximum concentration of the path lines near the tip of the blades in the upstream and downstream side of the rotor had occurred, which would be responsible for generation of maximum power coefficient in its clockwise rotation.

Keywords: two-bucket helical Savonius rotor, tip speed ratio, power coefficient, path line

Nomenclature

D	Overall rotor diameter
ρ	Density
d	Bucket diameter of the rotor
r	Bucket radius
h	Height of the Savonius rotor
μ	Viscosity
μ_t	Turbulent viscosity
e	Overlap
A	Swept area
T	Torque
u	Blade rotational speed
P_{rotor}	Power of the rotor
P_{max}	Maximum wind power

ω	Angular velocity
C_p	Power coefficient
λ	Tip speed ratio
V_{free}	Free stream velocity

1. Introduction

Wind energy is expected to play an increasingly important role in the future national energy scene (Fung, Scheffler, & Stolpe, 1981; Sesto & Casale, 1998). It has been estimated that roughly 10 million MW of energy are continuously available in the earth's wind. *Greenpeace* predicted that about 10% electricity could be supplied by the wind by the year 2020 and with the improved technology along with superior economics; experts predict wind power would capture 5% of the world energy market by the year 2020 (Joselin, Herberta, Iniyamb, & Sreevalsanc, 2007). In the last few decades many researchers had worked on the different designs of Savonius rotor and obtained its efficiency in the range of 15%-38% (Khan, 1975; Modi, Roth, & Fernando, 1984; Sharma, Gupta, Singh, & Singh, 2005; Biswas, Gupta, & Sharma, 2007). There had been some works done as to incorporate some modifications in the design of blades so that Savonius rotor may be quite useful for small-scale power requirements. Research conducted by Grinspan et al. (2001) in this direction led to the development of a new blade shape with a twist for the Savonius rotor. He reported a maximum power coefficient of 0.5. In the Continuation Saha et al. (1994) performed experiments on twist bladed Savonius rotor made of bamboo in a low-speed wind tunnel. They showed that their model was independent of wind direction and though the model produced slightly lower rotational speed but easy fabrication of such models made their design suitable for small-scale requirements. Further such design can worth hundred times better than those using deflecting plates & shielding to increase efficiency (Huda, 1992), which would make the design structurally complex. Again Saha and Rajkumar (2005) performed work on twist bladed metallic S-rotor and compared the performance with conventional semicircular blades having no twist. They obtain C_p of 0.14, which was higher than that of the later with C_p of 0.11. The rotor also produced starting torque and larger rotational speeds. Hassan et al. performed work computationally on twisted Savonius rotor. They present Computational Fluid Dynamics analysis of a Twisted Savonius rotor. Simulations were performed in a CFD software Flow-3D (Flow Science, Flow 3D version 10.0.), using Reynold's Averaged Navier-Stokes Equations (RANS) solver with structured rectangular mesh. They designed the rotor with 180° twist with two endplates and no central shaft. Further performance of the twisted Savonius rotor has been determined; this includes starting characteristics, static torque and rotational speed of the turbine. The Simulation results show better performance of twisted Savonius rotor as compared to the other conventional Savonius rotors. Zhao et al. (2009) investigated the performance of Savonius rotor based on numerical study, which was focused on the Improvement of power performance coefficient ($C_p = 0.15$) is low for conventional Savonius rotor. They introduced a new type-helical Savonius rotor, applies Computational Fluid Dynamics to analyze and improve the performance of the rotor from aspects ratio (H/D), number of blades, overlap distance and helical angle(θ). Their results shows that the performance coefficient of an optimum rotor reaches 0.2, when rotor has two blades and $H/D=6:1$, $e=0.3$, $\theta=180^\circ$; The starting torque is also better than that of conventional rotor. Their computation result also coincides well with their experimental results; this proves that the computation results are accurate. To decrease the variation of static torque in conventional Savonius rotors with rotor angle ranging from 0° to 360°, Kamoji et al. (2010) tested a helical rotor with a twist of 90°. They conducted experiments in an open-jet wind tunnel at gap ratios of 0.0, 0.05, and 0.08 to study the effect of the overlap ratio and the Reynolds numbers on its performance to evaluate the static torque, the dynamic torque, and the power coefficients. Morshed (2010) investigated the aerodynamic performance of three-bladed Savonius rotor, through wind tunnel experiments to find the aerodynamic characteristics like, drag coefficient, torque coefficient, and power coefficient of the rotor models with and without overlap at various Reynolds numbers. They compared its performance with and without a shaft between the end plates at different overlap ratios. A helical rotor without a shaft was also compared with the performance of the conventional Savonius rotor. They found that all helical rotors have a positive power coefficient of static torque for all rotor angles, but the rotors with a shaft had a lower power coefficient than those without. The power coefficient of the rotor without a shaft with a zero overlap ratio was marginally less than the conventional Savonius rotor. The rotor appeared to be sensitive to the Reynolds number, but this finding must be confirmed by rigorous experiments. Further, Bhaumik and Gupta (2010) studied experimentally the performance of helical Savonius rotor at 45° twist angle in a centrifugal blower. They consider the provision of different overlap ratio from 0.106 to 0.186. It is concluded from their result that maximum C_p is obtained as 0.421 at an overlap ratio of 0.147. Gupta and Deb (2011)

studied the CFD analysis of a two bucket helical Savonius rotor with shaft at 45° twist angle. From their study they concluded that the highest values of dynamic pressure and velocity magnitude were obtained at the chord ends with 45° bucket twist and 90° rotor angle, which would ensure improved performance of the rotor as a whole by increasing the aerodynamic torque production of the rotor.

Keeping this in view, a two-bucket helical Savonius rotor with shaft having 45° bucket twist angle was designed. Computational fluid dynamics analysis using Fluent software package (Fluent 6.2 documentation user's guide. 2005) was done to analyze the power coefficient of the helical Savonius rotor with shaft at 45° bucket twist angle at different rotor angles namely 0° , 45° , 90° , 135° and 180° . Analysis is also done at maximum tip speed ratio, variation of coefficient of power in a complete cycle of rotation from 0° to 360° in a step of 45° rotor angle. Further X-Y plots of tangential velocity and path lines for flow visualization at different angle is done to understand the flow physics of the rotor.

2. Geometry Model

The three-dimensional model of the two-bucket helical Savonius rotor with shaft at 45° twist angle is shown in Figure 1. Both the inner edge and the outer edge undergo a twist of 45° , a quarter pitch turn. The blade retains its semi-circular cross section from the bottom (0°) to the top (45°). The buckets were spaced 180° apart and were fixed to the central shaft with nut and bolt arrangements. The physical models were designed for five rotor angles namely 0° , 45° , 90° , 135° and 180° .

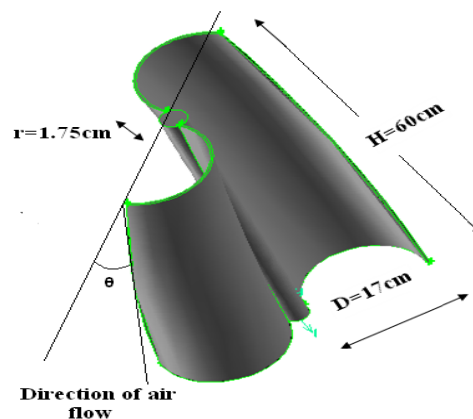


Figure 1. Helical Savonius rotor with shaft

3. Computational Model

3.1 Meshing Geometry and Boundary Condition

The designing of the computational mesh is done in Gambit 6.3.26 of the Fluent package. The computational domain of the rotor with the boundary conditions and the computational mesh for the rotor is shown in Figure 2 and 3. Velocity inlet and pressure outlet conditions were taken on the left and right boundaries respectively. The top and bottom boundaries of the computational domain had symmetry conditions on them. The buckets and the central shaft contained standard wall conditions. The computational mesh, composed of tetrahedral cells, is generated by placing the rotor in a box of dimensions $80\text{ cm} \times 80\text{ cm} \times 80\text{ cm}$ through which the air flow occurs.

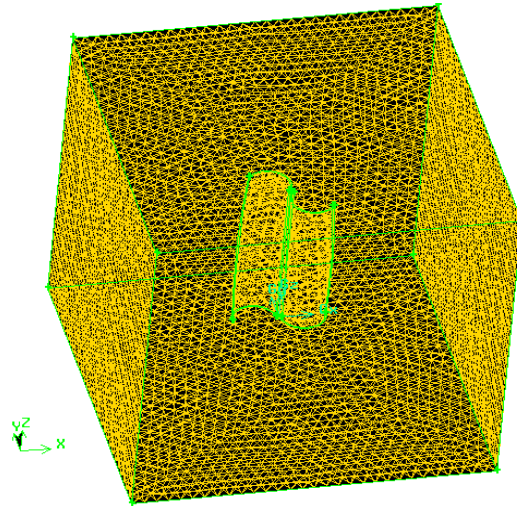


Figure 2. Computational mesh

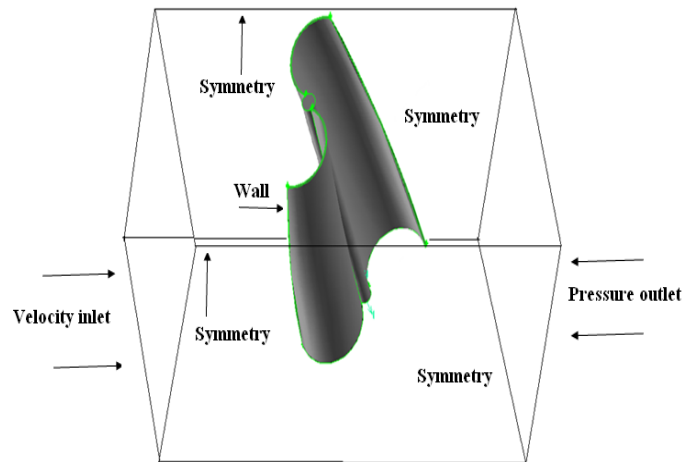


Figure 3. Computational domain with boundary condition

3.2 Turbulence Model

In this study Standard k- ϵ turbulence model has been used with logarithmic surface function in the analysis of turbulent flow. Momentum equation, x , y and z components of velocity, turbulent kinetic energy (k) and dissipation rate of turbulent kinetic energy (ϵ) have each been solved with the use of the program. All these equations have been solved by using the iteration method in such a way as to couple each equation in the central point of the cells, and second order interpolation method with a high reliability level has been employed. In the present study, the standard k- ϵ turbulence model with standard wall condition was used.

The standard k- ϵ equations can be represented as:

$$\frac{\partial}{\partial t}(\rho k) + \frac{\partial}{\partial x_i}(\rho k u_i) = \frac{\partial}{\partial x_j} \left[\left(\mu + \frac{\mu_t}{\sigma_k} \right) \frac{\partial k}{\partial x_j} \right] + G_k - \rho \epsilon - Y_M \quad (1)$$

$$\frac{\partial}{\partial t}(\rho \epsilon) + \frac{\partial}{\partial x_i}(\rho \epsilon u_i) = \frac{\partial}{\partial x_j} \left[\left(\mu + \frac{\mu_t}{\sigma_\epsilon} \right) \frac{\partial \epsilon}{\partial x_j} \right] + C_{1\epsilon} \frac{\epsilon}{k} (G_k) - C_{2\epsilon} \rho \frac{\epsilon^2}{k} \quad (2)$$

In these equations, G_k represents the generation of turbulence kinetic energy due to the mean velocity gradients.

Y_M represents the contribution of the fluctuating dilatation in compressible turbulence to the overall dissipation rate. $C_{1\varepsilon}$ and $C_{2\varepsilon}$ are constants. σ_k and σ_ε are the turbulent Prandtl numbers for k and ε , respectively. S_k and S_ε are user-defined source terms.

4. Analysis of Results

After the convergence of the solution, the power co-efficient (C_p) values are calculated for each value of input air velocity, rotor rotational speed and position of bucket at different rotor angle and tip speed ratios (λ). Following are the equations used to get the power coefficient.

$$\lambda = \frac{u}{v} = \frac{\pi dN}{60v} \quad (3)$$

$$T = F_T R = \frac{1}{2} \rho AV^2 C_T R = \frac{1}{4} \rho AV^2 C_T D \quad (4)$$

$$P_{rotor} = T\omega = \frac{2\pi NT}{60} \quad (5)$$

$$P_{max} = \frac{1}{2} \rho AV^3 \quad (6)$$

$$C_p = \frac{P_{rotor}}{P_{max}} \quad (7)$$

4.1 Variation of Power Coefficient at Different Rotor Angle

Figures (4.1-4.5) show below the maximum coefficient of power at different tip speed ratios (λ) whereas Figure 1.6 shows the variation of coefficient of power in a complete cycle of rotation (i.e. 0° to 360° in step of 45°). Tip speed ratio is defined as the ratio of blade rotational speed to the free stream velocity. Figure 4.1 shows at 0° rotor angle the maximum coefficient of power is obtained 0.0498 at a TSR of 1.636. Similarly Figure 4.2 shows at 45° rotor angle the maximum power coefficient is 0.4742 at a TSR of 1.636. For Figure 4.3, it is seen that for 90° rotor angle, the maximum power coefficient is around 0.3560 at a TSR of 1.636. At 135° rotor angle shown in Figure 4.4 the maximum power coefficient is obtained at 0.0216 at a TSR of 1.636. For Figure 4.5, it is seen that maximum power coefficient is obtained 0.04932 at a TSR of 1.636. Further at Figure 4.6 shows the variation of coefficient of power in a complete cycle of rotation at a maximum TSR of 1.636. The maximum power coefficient is obtained at 45° , 90° , 225° and 270° rotor angle while the worst one belongs to 0° , 135° , 180° and 315° .

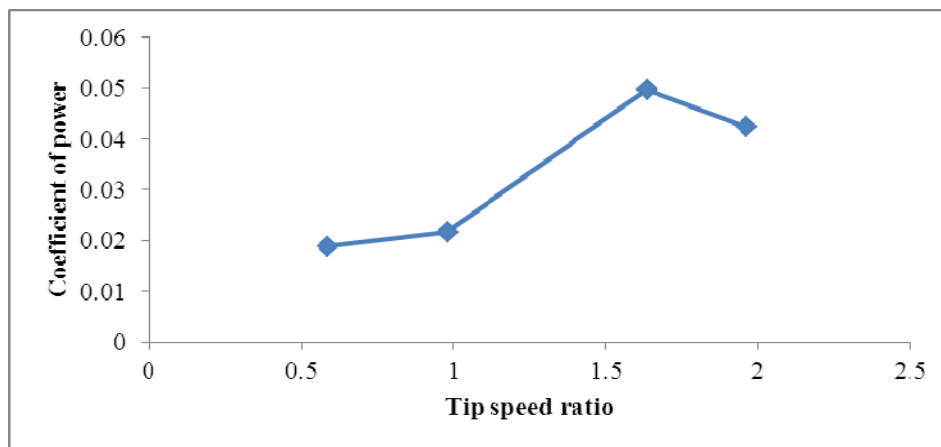


Figure 4.1. Variation of C_p at 0° rotor angle with TSR

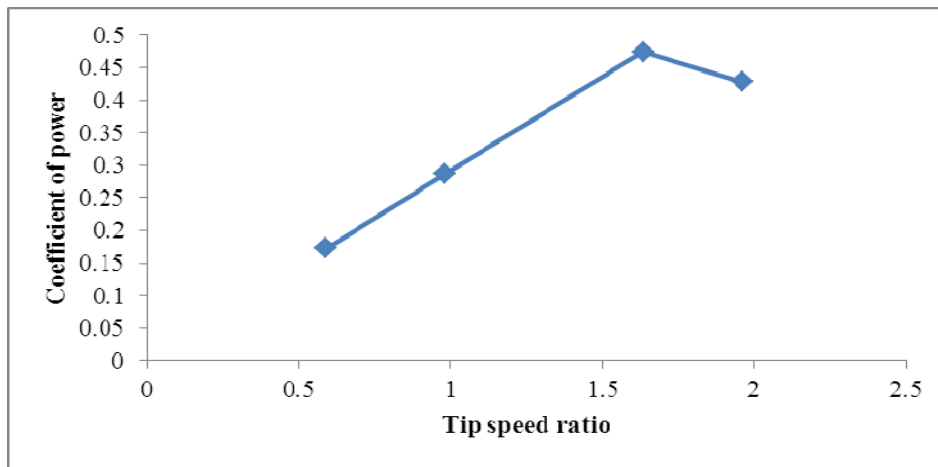


Figure 4.2. Variation of C_p at 45° rotor angle with TSR

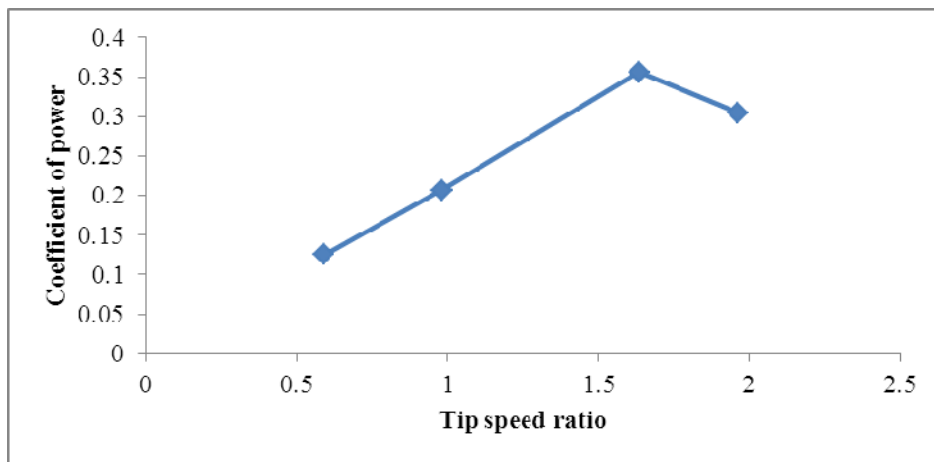


Figure 4.3. Variation of C_p at 90° rotor angle with TSR

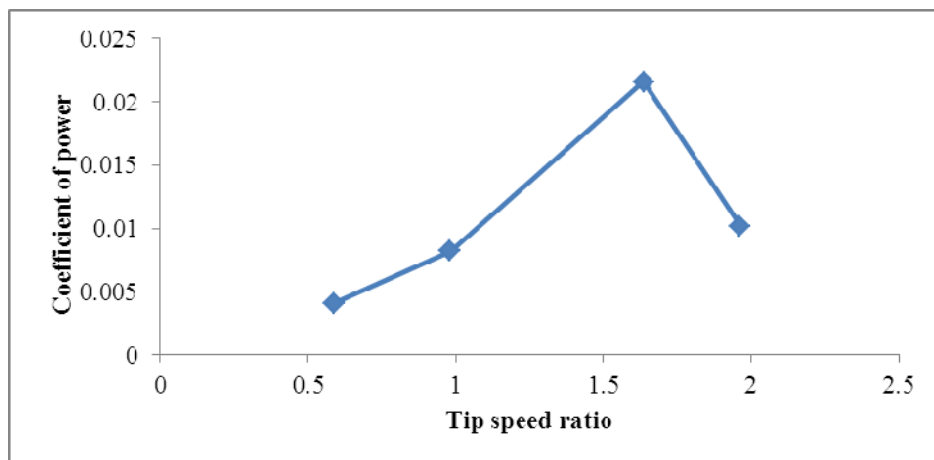


Figure 4.4. Variation of C_p at 135° rotor angle with TSR

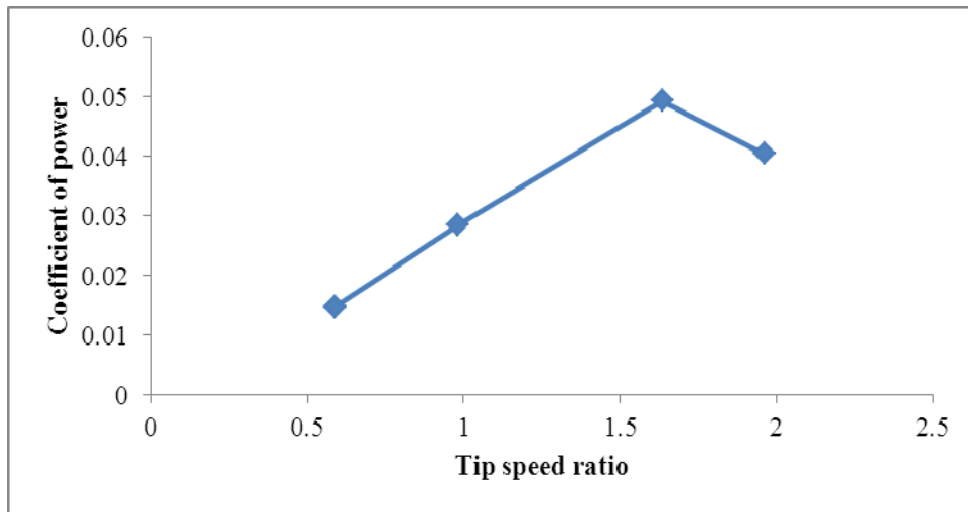


Figure 4.5. Variation of C_p at 180° rotor angle with TSR

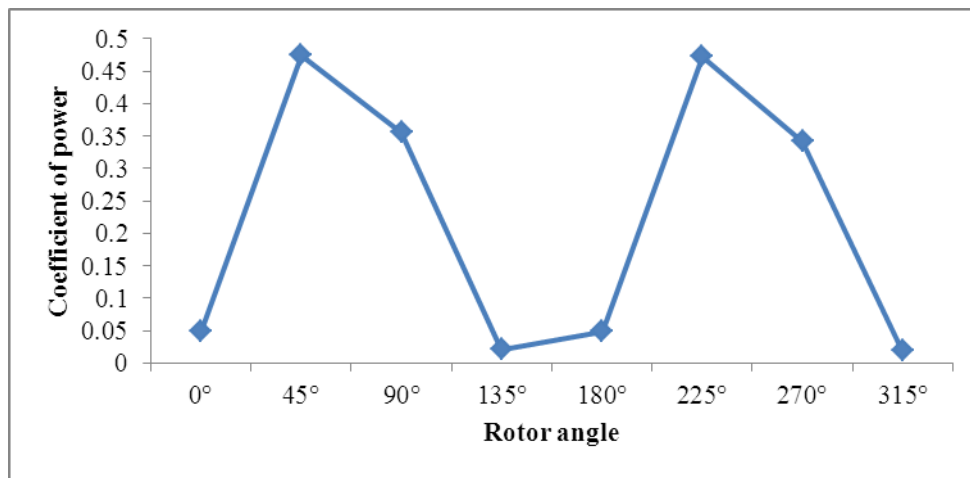


Figure 4.6. Variation of C_p at complete cycle of rotation at maximum $TSR=1.636$

4.2 X-Y Plot of Tangential Velocity

These plots are mainly two dimensional graphs that represent the variation of one dependent transport variable against another independent variable. The X-Y plots are the most precise and quantitative way to present the numerical data. X-Y plot of tangential velocity on surface located at centre of the wall are shown below in Figures 5.1-5.5. The variation of tangential velocity in different position from velocity inlet to the pressure outlet at the sweep surface i.e. at the centre of the wall is observed. The maximum change in tangential velocity will occur when the flow strikes the advancing bucket orthogonally and then the velocity gradually decreases in the downstream. Thus from the above XY plot it is shown that the maximum change in tangential velocity for helical Savonius rotor with shaft will occurs at 45° , 90° and 135° rotor angle while at 0° and 180° rotor angle the change in tangential velocity is approximately same. Hence it is concluded from XY plot analysis of tangential velocity that the performance of helical Savonius rotor with shaft produces maximum power at 45° , 90° and 135° rotor angle where the maximum change in tangential velocity across the rotor occurs.

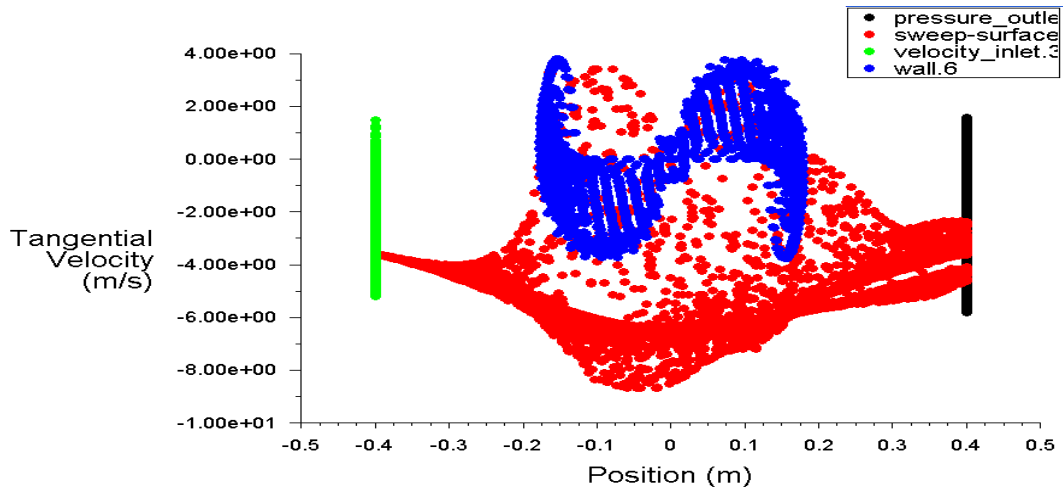


Figure 5.1. Tangential velocity Vs Position at 0° rotor angle (Plot direction X1, Y0, Z0)

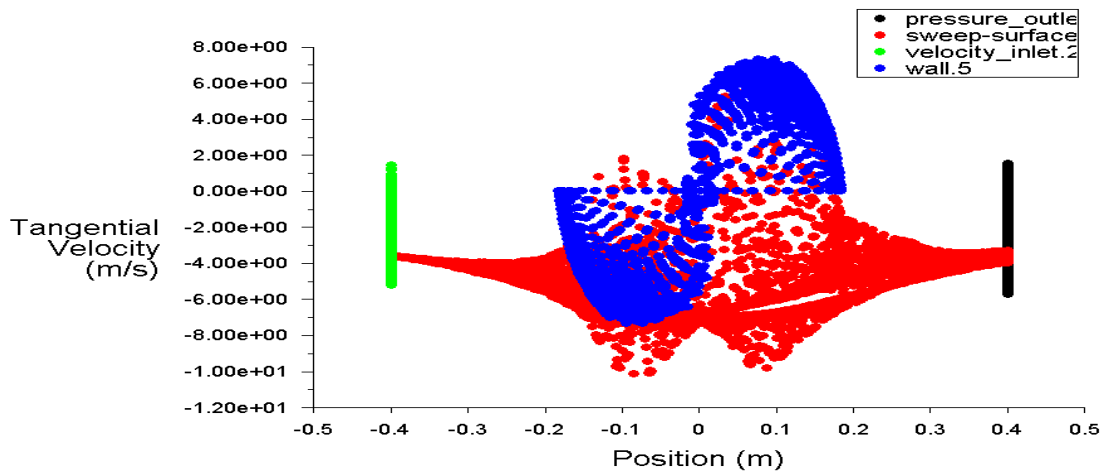


Figure 5.2. Tangential velocity Vs Position at 45° rotor angle (Plot direction X1, Y0, Z0)

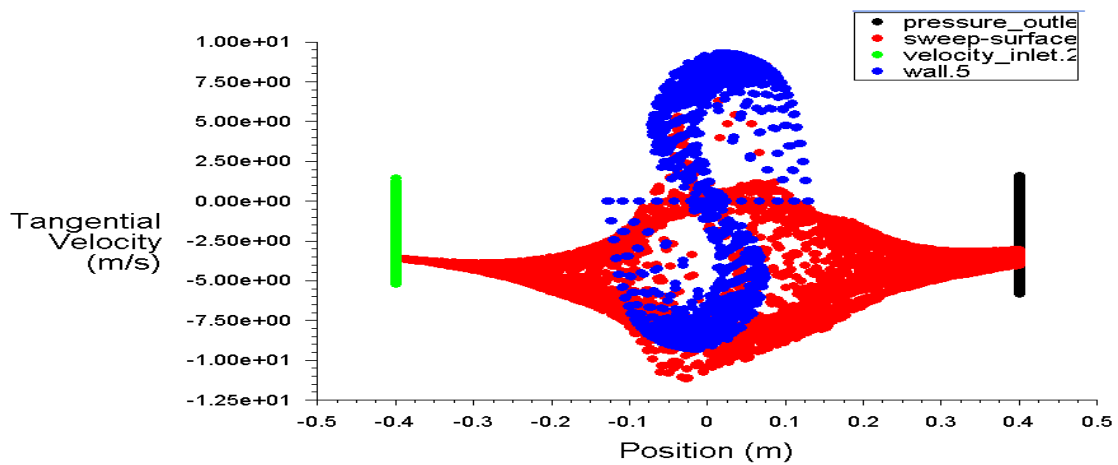


Figure 5.3. Tangential velocity Vs Position at 90° rotor angle (Plot direction X1, Y0, Z0)

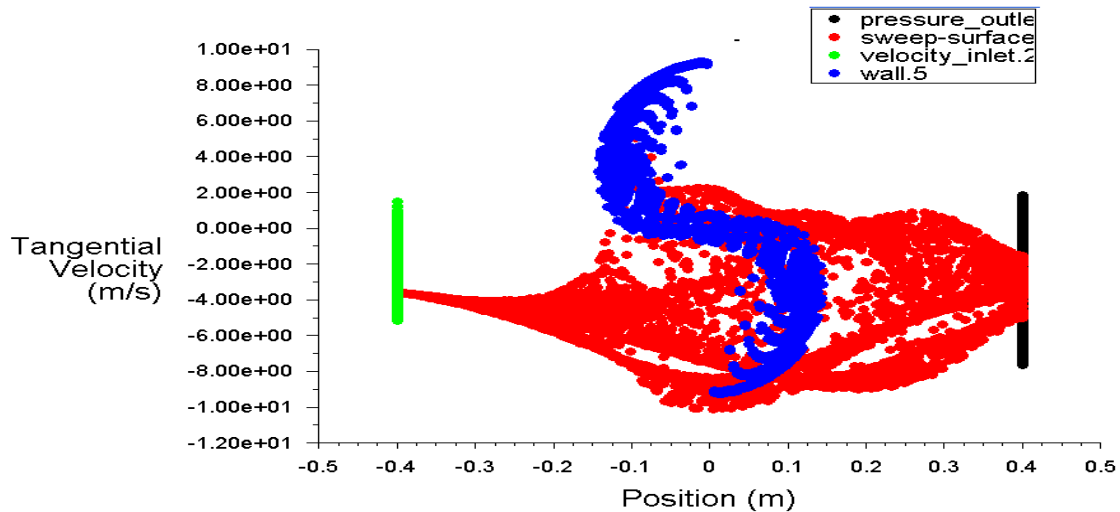


Figure 5.4. Tangential velocity Vs Position at 135° rotor angle (Plot direction X1, Y0, Z0)

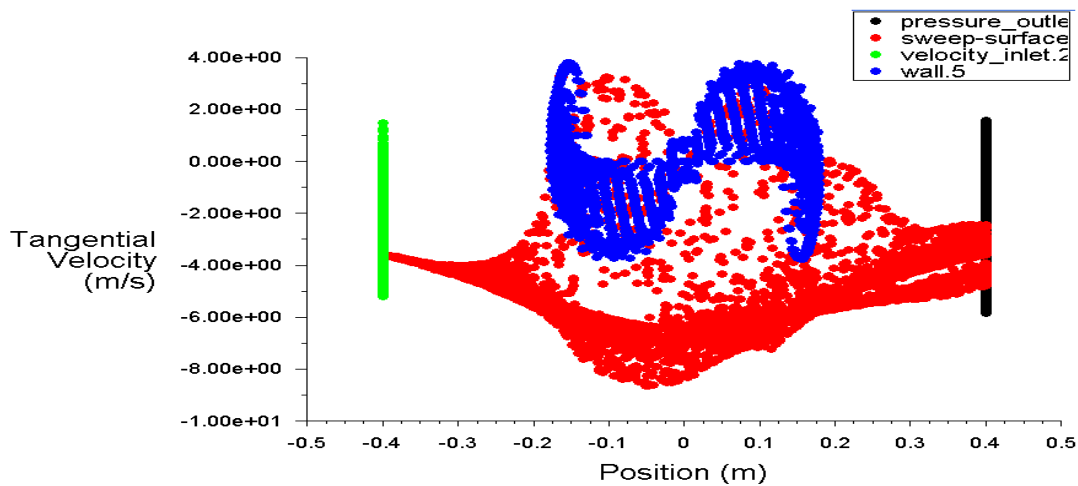
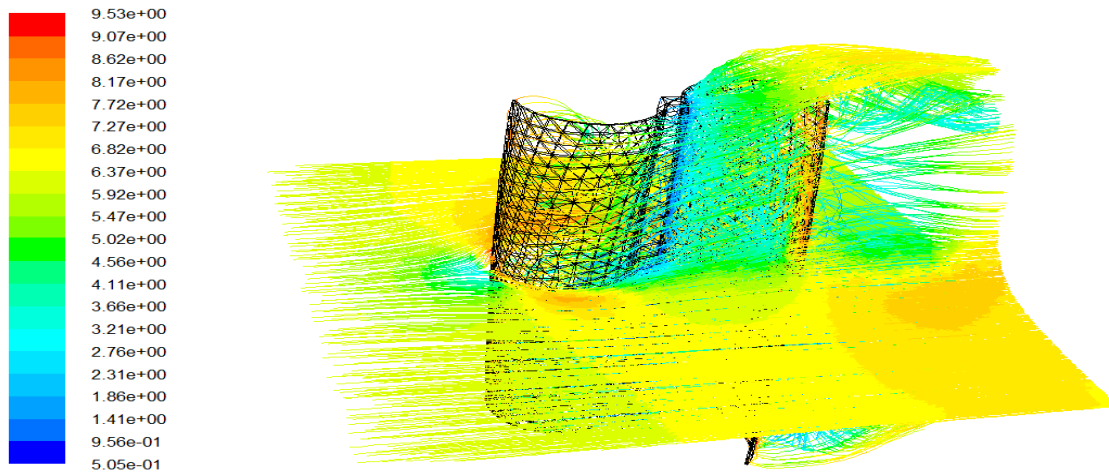


Figure 5.5. Tangential velocity Vs Position at 180° rotor angle (Plot direction X1, Y0, Z0)

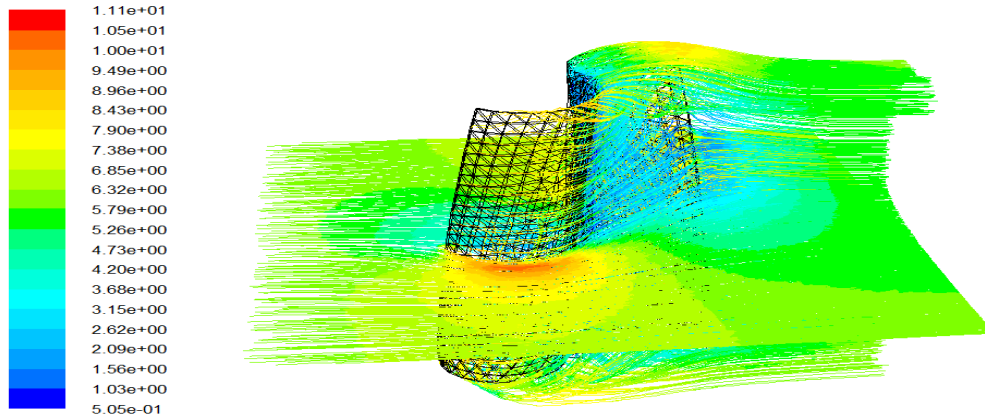
4.3 Path Lines across the Rotor

Path lines are used to visualize the flow of mass less particles in the problem domain. The fluid motion in computational domain is described by tracing the kinematic behavior of each and every individual particle constituting the flow. Figures 6.1 to 6.5 shows the path followed by a fluid particle from velocity inlet to pressure outlet while in motion. The path lines at the sweep surface of the plane perpendicular to the rotor axis at a distance $x = 0$, $y = 1$ and $z = 0$ are shown for 0° , 45° , 90° , 135° and 180° respectively. When bucket position is at 45° , 90° and 135° rotor angles, maximum concentration of the path lines towards the tip of the blade at the upstream and downstream side of the rotor occurs, which is responsible for generation of higher aerodynamic torque for producing maximum power. While at 0° and 180° rotor angle significant flow separation occurs and hence power coefficient is less at this rotor angle.



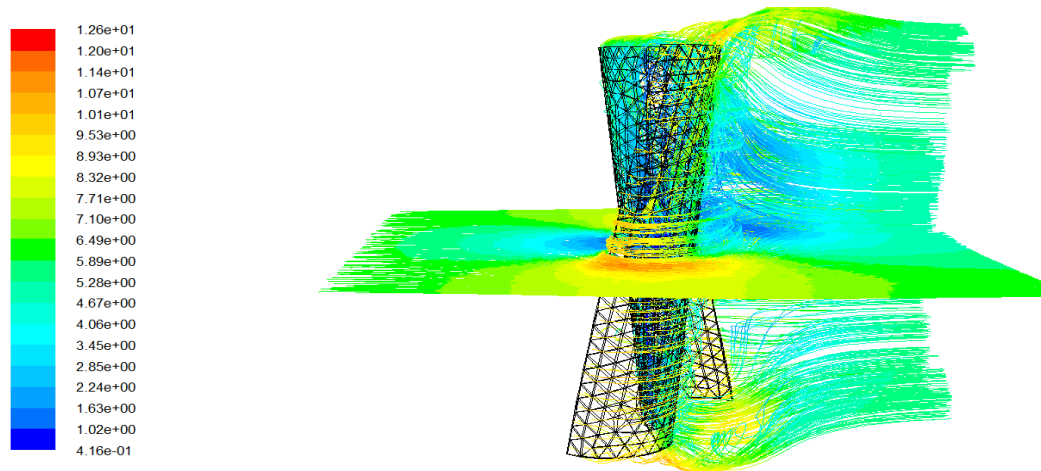
Pathlines Colored by Velocity Magnitude (m/s)

Figure 6.1. Path line at 0° Rotor Angle



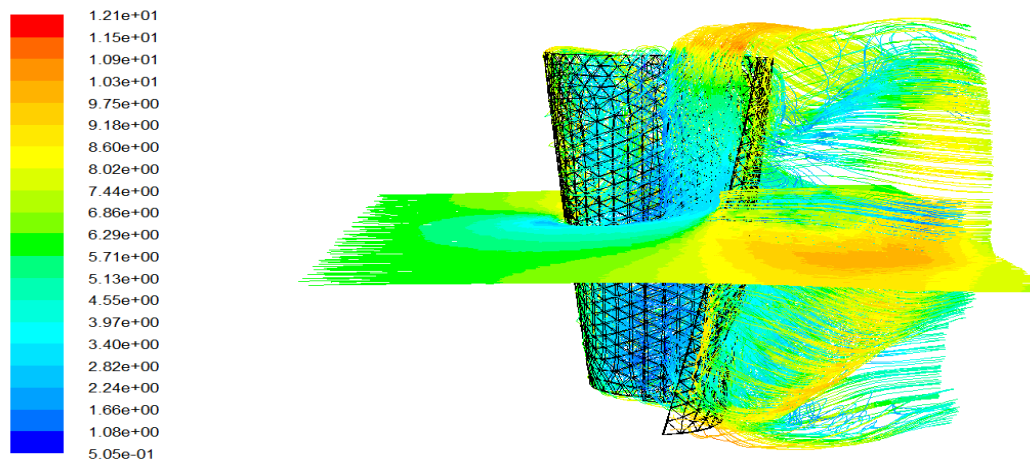
Pathlines Colored by Velocity Magnitude (m/s)

Figure 6.2. Path line at 45° Rotor Angle



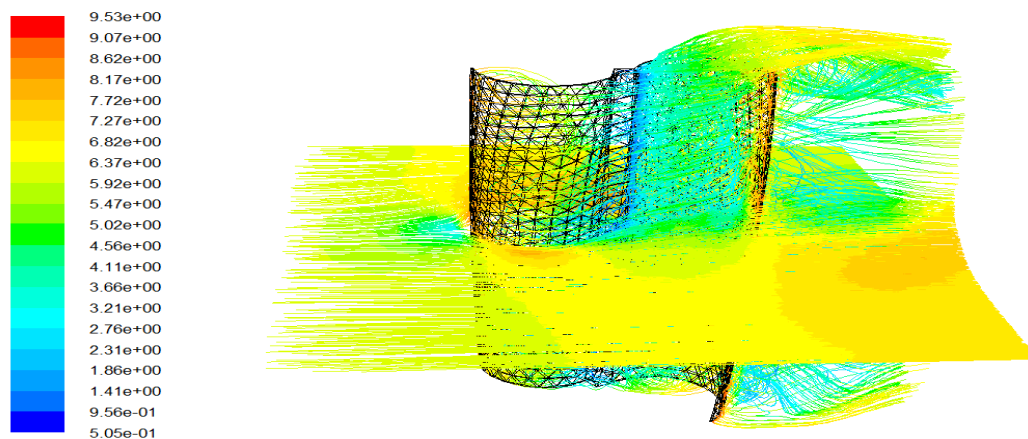
Pathlines Colored by Velocity Magnitude (m/s)

Figure 6.3. Path line at 90° Rotor Angle



Pathlines Colored by Velocity Magnitude (m/s)

Figure 6.4. Path line at 135° Rotor Angle



Pathlines Colored by Velocity Magnitude (m/s)

Figure 6.5. Path line at 180° Rotor Angle

5. Conclusion

The performance of a helical Savonius rotor with shaft at 45° bucket twist angle for one complete cycle of rotation was analyzed using Fluent CFD software. From the study, the following conclusions are summarized:

- 1) The power coefficient (C_p) increases with the increase in tip speed ratio up to a certain limit i.e. 1.636 and then decreases with further increase in tip speed ratio. Therefore there is an optimum tip speed ratio at which C_p is the maximum.
- 2) The power coefficient obtained at all the rotor angles is positive. Thus at all rotor angle positive power coefficient is obtained from the rotor. And higher values of C_p are obtained in the advancing stroke of rotation from 45° upto 110° and in the return stroke of rotation beyond 180° upto 270°, thus contributing to maximum power production by the rotor in these range of angles, which is also corroborated from the analysis of tangential velocity distribution across the rotor at these rotor angles.
- 3) From XY plot it is shown that the maximum change in tangential velocity for helical Savonius rotor with shaft will occur at 45°, 90° and 135° rotor angle to produce maximum positive tangential thrust while at 0° and 180° rotor angle the change in tangential velocity is approximately same.
- 4) Path lines for flow past the rotor shows its higher concentration near the tip of the blades in the upstream and downstream side of the rotor, which is responsible for generation of maximum power coefficient in its clockwise rotation.

References

- Bhaumik, T., & Gupta, R. (2010). Performance measurement of a two bladed helical Savonius rotor. *Proceedings of the 37th International & 4th National Conference on Fluid Mechanics and Fluid Power, FMFP2010*, December 16-18, 2010, IIT Madras, Chennai, India.
- Biswas, A., Gupta, R., & Sharma, K. K. (2007). Experimental Investigation of Overlap and Blockage Effects on Three-Bucket Savonius Rotors. *Wind Engineering*, 31(5), 363-368. <http://dx.doi.org/10.1260/030952407783418702>
- Fluent 6.2 documentation user's guide. (2005).
- Fung, K. T., Scheffler, R. L., & Stolpe, J. (1981). Wind energy a utility perspective. *IEEE Trans Power Appar System*, 100, 1176-82. <http://dx.doi.org/10.1109/TPAS.1981.316586>
- Grinspan, A. S., Kumar, P. S., Mahanta, P., Saha, U. K., Rao, D. V. R., & Bhanu, G. V. (2001). Design, development & testing of Savonius wind turbine rotor with twisted blades. *Proc. of 28th National Conference on Fluid Mechanics and Fluid Power*, Chandigarh, Dec 13-15, pp. 428-431, 2001.
- Gupta, R., & Deb, B. (2011). CFD analysis of a two-bucket helical Savonius rotor with shaft at 45° twist angle. *Sharjah International Symposium of Nuclear and Renewable Energies for 21st Century (SHJ-NRE11)*, April 3-5, 2011, College of Sciences, University of Sharjah UAE.
- Hassan, Md. I., Iqbal, T., Khan, N., Hinchey, M., & Masek, V. (2010). *CFD Analysis of a Twisted Savonius Turbine*. Memorial University of Newfoundland.
- Huda, M. D. (1992). The performance of an S-shaped Savonius rotor with a deflecting plate. *RERIC International Energy Journal*, 14, 25-32.
- Joselin, G. M., Herberta, S., Iniyamb, Ã., & Sreevalsanc, E. (2007). A review of wind energy technologies. Renewable and Sustainable Energy Reviews. *Renewable and Sustainable Energy Reviews*, 11, 1117-1145. <http://dx.doi.org/10.1016/j.rser.2005.08.004>
- Kamoji, M. A., Kedare, S. B., Prabhu, S. V. (n.d.). Performance tests on helical Savonius rotors. *International Journal on Renewable Energy*, 34, 521-529.
- Khan, M. H. (1975). *Improvement of Savonius Rotor-windmill* [M.S. thesis]. University of the Phillipines, Lasbonas.
- Modi, V. J., Roth, N. J., & Fernando, M. S. U. K. (1984). Optimal configuration studies and prototype design of a wind energy operated irrigation system. *Journal of Wind Engg & Industrial Aerodynamics*, 16, 85-96. [http://dx.doi.org/10.1016/0167-6105\(84\)90050-3](http://dx.doi.org/10.1016/0167-6105(84)90050-3)
- Morshed, K. N. (2010). *Experimental and numerical investigations on aerodynamic characteristics of Savonius wind turbine with various overlap ratios* [M.S. thesis]. Statesboro, Georgia.
- Saha, U. K., & Rajkumar, M. (2005). On the performance analysis of Savonius rotor with twisted blades. *Journal of Renewable Energy*, 31, 0960-1481.
- Saha, U. K., Mahanta, P., & Grispan, A. S. (1994). Twisted bamboo bladed rotor for Savonius wind turbines. *Journal of Solar Energy Society of India*, 14(2), 1-10.
- Sesto, E., & Casale, C. (1998). Exploitation of wind as an energy source to meet the world's electricity demand. *Wind Eng.*, 74-76, 375-387.
- Sharma, K. K., Gupta, R., Singh, S. K., & Singh, S. R. (2005). Experimental investigation of the characteristics of a Savonius wind turbine. *Wind Engineering*, 29(1), 77-82. <http://dx.doi.org/10.1260/0309524054353674>
- Zhao, Z. Z., Zheng, Y., Xu, X. Y., & Hu, G. X. (2009). Research on the Improvement of the Performance of Savonius Rotor Based on Numerical Study. In *Sustainable Power Generation and Supply, 2009. SUPERGEN '09. International Conference on 6-7 April, 2009*.